A 2-pyridone modified zinc phthalocyanine with three-in-one multiple functions for photodynamic therapy

Yanqing Li [‡a], Chongchong Wang [‡a], Lin Zhou [a,*], Shaohua Wei [a,b,*]

[a] College of Chemistry and Materials Science, Jiangsu Key Laboratory of Biofunctional Materials, Jiangsu Collaborative Innovation Centre of Biomedical Functional Materials, Key Laboratory of Applied Photochemistry, Nanjing Normal University, Nanjing, Jiangsu 210023, China.

[b] School of Chemistry and Chemical Engineering, Yancheng Institute of Technology, Yancheng, Jiangsu 224051, China.

E-mail: zhoulin@njnu.edu.cn (L. Zhou), shwei@njnu.edu.cn (S. H. Wei).

[‡] Y.Q. Li and C.C. Wang contributed equally to the work.

Experimental Section

Chemicals

The water used in the experiment was double distilled water, and the reagents and chemicals were not further purified. 1-(bromomethyl)-4-nitrobenzene, pyridin-2(1H)-one, N-(3-dimethylamino-propyl)-N-ethyl carbodiimide hydrochloride (EDC·HCl), 1-Hydroxybenzotriazole (HOBT), Cremophor® EL (CrEL), Pd/C, DCM were purchased from Aladdin (China). K_2CO_3, Na_2CO_3, CH_3CN, Na_2SO_4, NaOH, $NaHCO_3$, NaCl, KCl, $Na_2HPO_4{\cdot}12H_2O$, KH_2PO_4, dichloromethane (DCM), petroleum ether (PE), ethyl-acetate (EA), dimethylformamide (DMF) were purchased from Sinopharm Chemical Reagent Co. Ltd. CH_3OH was obtained from Wuxi Yasheng Chemical Co. LTD. Ethylene diamine tetra acetic acid (EDTA), Tris, 3-[4,5-dimethylthiazol-2-yl]-2,5-diphenyltetrazolium bromide (MTT), a disodium salt of 9,10-anthracenedipropionic acid (ADPA) were obtained from Sigma-Aldrich (USA). Newborn calf serum (NCS) was purchased from Hangzhou Sijiqing Institute of Biomaterials. 2,7-dichlorodihydrofluorescein diacetate (DCFH-DA), singlet oxygen sensor green reagent (SOSG), and Dulbecco's Modified Eagle Media (DMEM) were obtained from Thermo Fisher (USA). Annexin V-FITC apoptosis detection kit was purchased from Shanghai Yeasen biotechnology Co. Ltd (China). Glycine, sodium lauryl sulphate was bought from Sangon Biological Engineering (Shanghai) Co. LTD. BCA kit, ECL kit, cell lysis buffer for Western and IP, SDS-PAGE sample loading buffer, polyvinylidene fluoride (PVDF) membrane (0.45 μm)

were bought from Beyotime (China). HIF-1α antibody was obtained from Cell Signaling Technology (CST). The primary antibody of glyceraldehyde-3-phosphate dehydrogenase (GAPDH), peroxidase affinipure goat anti-rabbit IgG (H+L) were obtained from Shanghai Yeasen Biotechnology Co. Ltd (China).

Instrument

The particle size and distribution were recorded by H-7650 microscopy with 80 kV accelerating voltage (Hitachi, Japan) and MALVERN NANO-ZS90 laser particle size analyzer (Malvern, UK). UV-vis absorption spectra were measured using a Cary 50 spectrophotometer (Varian, USA). ^{13}C nuclear magnetic resonance spectra and ^{1}H nuclear magnetic resonance spectra were determined with the AN-400 MHz NMR instrument (Bruker, Germany). Mass spectra measurements were measured with the MALDI-TOF-MS (Bruker, Germany) or ESI-MS. Fluorescence spectra were obtained with a Cary Eclipse fluorescence spectrophotometer (Varian, USA). Transmission electron microscopy images were observed under JEM-2100 microscopy (Hitachi, Japan). The absorbance of formazan in MTT assay was determined by a multifunctional enzyme marker (Tecan Spark 10 M). Fluorescence images in the cells were qualitatively observed under confocal laser scanning microscopy (Nikon Eclipse Ti). Fluorescence intensity and Cell apoptosis were quantitatively detected by flow cytometry (Beckman Coulter Epics XL-MCL, USA). The content of C, H, O and N in ZnPc-PYR were determined with the Elementar Vario EL cube.

Synthesis of 1-(4-nitrobenzyl) pyridin-2(1H)-one.

The 1-(bromomethyl)-4-nitrobenzene (2.3 g, 10.5 mmol), pyridine-2(1H)-one (1 g, 10.5 mmol), and K_2CO_3 (2.9 g, 21 mmol) were added into CH_3CN (20 mL) under a nitrogen atmosphere at 80 °C overnight with the blender on low. The reaction products were dissolved in DCM, washed with water several times after reaction, the reaction mixture was concentrated under reduced pressure and mixed with water (10 mL), dried over anhydrous Na_2SO_4. Finally, the purification was carried out by column chromatography (PE/EA = 5/1, DCM/MeOH = 100/1, v/v). The product was vacuum dried overnight, and 1.8 g yellow solid product was recovered. ^{1}H NMR (400 MHz, d_6-DMSO), δ (ppm) 8.22 (d, J = 8.8 Hz, 2H), 7.86 (dd, J_{12} = 2.0 Hz, J_{23} = 6.8 Hz, 1H), 7.53-7.44 (m, 3H), 6.45 (d, J = 8.8 Hz, 1H), 6.30 (td, J_{12} = 1.6 Hz, J_{23} = 5.2 Hz, 1H), 5.24 (s, 2H). ^{13}C NMR (100 MHz, d_6-DMSO): δ (ppm) 161.88, 147.27, 145.54, 140.96,

139.73, 129.06, 124.16, 123.86, 120.45, 106.29, 51.41. MS-ESI (m/z): calculated for $C_{12}H_{10}N_2O_3$ 230.07. Found $[M - H]^-$ 229.0.

Synthesis of 1-(4-aminobenzyl) pyridin-2(1H)-one.

The 1-(4-nitrobenzyl) pyridine-2(1H)-one (1 g, 4.3 mmol), $HCOONH_4$ (1.5 g, 23.8 mmol) and Pd/C (150 mg, 10 %) were diluted in MeOH (20 mL) under a N_2 atmosphere at room temperature for 6 h. Under the condition of CH_3OH as an eluent, the purification of reaction mixture was carried out and the solvent was evaporated under reduced pressure. The white solid residue was dissolved in DCM, washed with Na_2CO_3 several times, and the mixed solution was still extracted with DCM. The extracts were dried over anhydrous Na_2SO_4 and then filtered. The evaporated affording product as a yellow solid. ^{1}H NMR (400 MHz, d_6-DMSO), δ (ppm) 7.69 (dd, J_{12} = 2.4 Hz, J_{23} = 6.8 Hz, 1H), 7.41-7.34 (m, 1H), 7.02 (d, J = 8.4 Hz, 2H), 6.50 (d, J = 8.4 Hz, 2H), 6.38 (dd, J_{12} = 0.8 Hz, J_{23} = 8.4 Hz, 1H), 6.19 (td, J_{12} = 1.2 Hz, J_{23} = 5.6 Hz, 1H), 5.22-5.00 (m, 2H), 4.88 (s, 2H). ^{13}C NMR (100 MHz, d_6-DMSO): δ (ppm) 161.83, 148.65, 140.15, 139.23, 129.68, 124.70, 120.18, 114.22, 105.76, 51.09. MS-ESI (m/z): calculated for $C_{12}H_{10}N_2O_3$ 200.09. Found $[M - H]^-$ 201.2.

Synthesis of ZnPc-PYR and ZnPc-BZA.

The synthetic route of ZnPc-PYR was illustrated in the Figure S1.

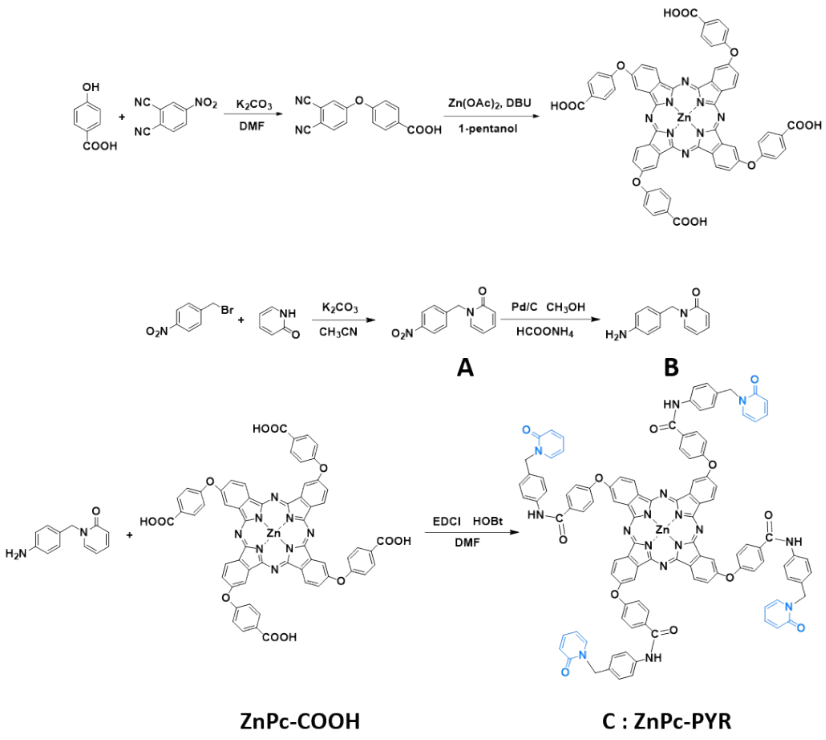

Fig. S1. Synthesis route of ZnPc-PYR.

The synthetic route of 2,9,16,23-4-(carboxyl phenoxy) ZnPc-COOH has been published in the previous report of our research group. [1] ZnPc-COOH (56 mg, 50 μM), EDC·HCl (76.68 mg, 400 μM) and HOBt (54.05 mg, 400 μM) were evenly mixed in DMF (5 ml), and the mixture was stirred for 1 h at 25 °C. In an ice-water bath, the abovementioned mixture was dropped into 1-(4-aminobenzyl) pyridin-2(1H)-one (80 mg, 400 μM) solution (2 mL DMF). After that, the reaction was continued for 1 h at 0°C. The mixture was then added to acetone (80 mL) and centrifuged to collect the precipitate. Dissolve the crude solid in an acidic aqueous solution (pH = 4), take the supernatant after centrifugation, and adjust the pH to 10 with10 % (wt %) NaOH. The solid product was purified by centrifugation again, and washed several times with EA. Then, ZnPc-PYR (36.2 mg) was afforded by vacuum-drying. ^{1}H NMR (400 MHz, d_6-DMSO): δ (ppm) 10.32 (dd, J_{12} = 6.4 Hz, J_{23} = 25.6 Hz, 4H), 9.04-8.36 (m, 12H), 8.20 (d, J = 34.4 Hz, 8H), 7.79 (s, 16H), 7.47-7.20 (m, 16H), 6.44 (d, J = 8.8 Hz, 4H), 6.25 (s, 4H), 5.08 (s, 8H). ^{13}C NMR (100 MHz, d_6-DMSO): δ (ppm) 165.14, 162.79, 161.90, 161.75, 160.52, 160.33, 157.35, 140.49, 139.65, 139.47, 139.10, 133.77, 133.02, 133.60, 128.68, 124.34, 121.01, 120.33, 118.92, 118.54, 106.01, 51.19. Anal. Calcd for $C_{108}H_{72}N_{16}O_{12}Zn$: C, 70.07; H, 3.92; O, 10.37, N, 12.12. Found: C, 69.90; H, 4.115; O, 10.626, N, 11.97.

The synthetic route of ZnPc-BZA was illustrated in the supporting information and Figure S2. ZnPc-

COOH (56 mg, 50 μM), EDC·HCl (76.68 mg, 400 μM), and HOBt (54.05 mg, 400 μM) were evenly mixed in 5 mL of DMF and kept for 1 h at 25 °C. In an ice−water bath, the abovementioned mixture was dropped into 4-benzylaniline (73.3 mg, 400 μM) solution (2 mL DMF). After that, the reaction was continued for 1 h at 0 °C. The mixture was then added to acetone (80 mL) and centrifuged to collect the precipitate. Dissolve the crude solid in an acidic aqueous solution (pH = 4), take the supernatant after centrifugation, and adjust the pH to 10 with 10 % (wt %) NaOH. The solid product was purified by centrifugation again, and washed several times with EA. Then, ZnPc-BZA (36.2 mg) was afforded by vacuum-drying. ^{1}H NMR (400 MHz, d6-DMSO): δ (ppm) 10.29 (dd, J_{12} = 8.8 Hz, J_{23} = 31.6 Hz, 4H), 8.77 (d, J = 24.0 Hz, 4H), 8.51-8.02 (m, 12H), 7.88-7.47 (m, 20H), 7.24 (qd, J = 14.5, 6.9 Hz, 28H), 5.08 (s, 8H). ^{13}C NMR (100 MHz, d6-DMSO): δ (ppm) 165.07, 160.48, 141.97, 139.55, 137.70, 137.03, 136.93, 133.63, 130.76, 130.64, 129.32, 129.29, 129.10, 128.88, 126.39, 124.30, 121.12, 118.50, 77.36, 44.82. MS-MALDI-TOF (m/z): calculated for $C_{112}H_{76}N_{12}O_8Zn$: 1780.52. Found: 1781.18.

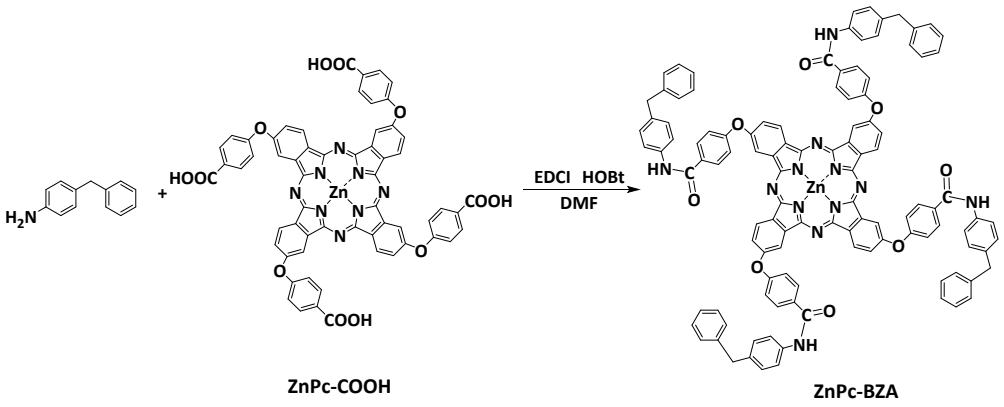

Fig. S2. The synthetic route of ZnPc-BZA.

Extracellular ROS Detection

DCFH was used as a trapping molecule to detect the total ROS generation. DCFH was obtained by hydrolysis of DCFH-DA in DMSO in the presence of NaOH (0.1 M, 2 mL). Photosensitizers solution ([ZnPc-PYR] = 6 μM) was mixed with DCFH (0.1 mM) in aqueous solution that contained 0.001 % CrEL and irradiated by light. The fluorescence spectrophotometer monitored the 475 nm fluorescence intensity changes of DCFH (slit width: d_{ex} = 10 nm, d_{em} = 10 nm). 665 nm LED groups: 0.4 W cm^{-2}, the fluorescence signal intensity was detected once every 5 s. 808 nm LED groups: 0.25 W cm^{-2}, the fluorescence signal intensity was detected once every 1 min.

$^{1}O_2$ generation of drugs was also detected with ADPA (100 μM) in this mixture after irradiated by 665

(0.4 W cm^{-2}), and 808 nm (0.25 W cm^{-2}) light and the 378 nm absorbance intensity decreasing was monitored once every 30 s.

Storage and release of $^1O_2$

In order to verify the feasibility of continuous $^1O_2$ release of ZnPc-PYR under non-light conditions, we used the commercial singlet oxygen probe ADPA to detect this process. $^1O_2$ can react with ADPA to produce the corresponding endogenous peroxide, which induces ADPA to bleach and reduces its absorbance intensity at 378 nm. ADPA can be used as a capture agent for singlet oxygen. A far better plan was that ZnPc-BZA (without singlet oxygen release unit) was synthesized as a parallel intervention group. Before running the detection, ZnPc-PYR, ZnPc-BZA ([ZnPc-PYR] = [ZnPc-BZA] = 10 μM) were dissolved in aqueous solutions of 0.001 % CrEL, respectively, and then mixed ADPA at 100 μM, and 665 nm LED (0.4 W cm^{-2}) was used as excitation light source. The absorbance spectra of ADPA at 378 nm were recorded at different time-intervals (After 30 s of light irradiation, avoid light for 30 min at 37 °C. This cycle was conducted 4 times).

In vivo and in vitro experiments

Murine mammary carcinoma cells (4T1 cells) and human cervical carcinoma cells (HeLa cells) were purchased from the cell bank of the Chinese Academy of Sciences (Shanghai, China). The cells were cultured in DMEM with 10 % (v/v) NBS in the incubator (5 % CO_2, 37 °C). SPF laboratory animals were purchased from Hangzhou Ziyuan Laboratory Animal Technology Co., Ltd. All animal experiments were performed under the approval of the China Animal Ethics Committee of Nanjing Normal University guidelines. All animal experiments followed the China Animal Ethics Committee of Nanjing Normal University's institutional guidelines and performed following the regulations for the Administration of Affairs Concerning Experimental Animals of China.

Western blotting

The hypoxia preconditioning of HeLa cells was performed in a hypoxic incubator (1 % O_2, 5 % CO_2, 37 °C). After 24 hours of cultured, the cells were colocalized with serum-free medium (control group), ZnPc-PYR (6 μM), CrEL (0.001 %), DMSO (6 μL) for 4 hours. As HIF-1α was rapidly degraded in the presence of both oxygen and iron, Cell lysis buffer and PBS that contained EDTA (5 mM) to lower the iron content in HeLa cells to inhibit HIF-1α degradation. Equivalent protein samples (5 μg) were

subjected to SDS-PAGE electrophoresis under a constant voltage and transferred to the PVDF membrane (0.45 μM) under constant current. PVDF membranes were immersed in a blocking solution (5 % low-fat milk) and shocked for an hour at room temperature. Each section was incubated with primary antibody (HIF-1α, GAPDH) overnight at 4 °C and then incubated with a secondary antibody for an hour. Eventually, according to the directions, the washed membranes were carried out using the ECL kits.

Intracellular ROS Detection

ROS in cells could oxidize DCFH without fluorescence to produce DCF with fluorescence. The green fluorescence intensity was proportional to the level of ROS.

We compared the ROS production capacity of ZnPc-PYR under 665 and 808 nm light irradiation and conducted experiments under the same light dose conditions. HeLa cells were cultured in Laser confocal Petri dishes overnight and co-incubated with ZnPc-PYR (6 μM) for 4 hours. After that, HeLa cells were incubated with 5 μM of DCFH-DA fluorescent probe for 1 hour and exposed to light at 665 nm (1 W cm^{-2}, 2 min) or 808 nm (1 W cm^{-2}, 2 min) to detect the intracellular ROS for 665 or 808 nm groups, respectively. The green fluorescence signal in HeLa cells was observed using CLSM at the maximum excitation wavelength of 488 nm and the maximum emission wavelength of 525 nm. For 665 + 808 nm group, HeLa cells were incubated with 5 μM of DCFH-DA fluorescent probe for 1 hour and exposed to light at 665 nm (1 W cm^{-2}, 2 min) and 808 nm (1 W cm^{-2}, 2 min). We use the pork to simulate the treatment of deep tumors. When lighting is performed, a piece of pork muscle tissue with an average thickness of 1.5 cm is placed in parallel in front of the 808 nm excitation light source (808 nm laser: 1 W cm^{-2}, 2 min) to simulate deep tumors' treatment.

Storage and release of $^1O_2$ in vitro

To verify the capacity of continuous release of $^1O_2$ in the absence of light, we monitored this process by flow cytometry or CLSM. After the HeLa cells were cultured in 6-well plates or Laser confocal Petri dishes overnight, the medium was replaced, and the HeLa cells were stained with SOSG (5 μM) for one hour after co-incubated with ZnPc-PYR for 4 h and irradiated by 665 nm laser for 3 min, 808 nm laser for 15 min. After keeping under dark for 6 h, The green fluorescence signal was detected after washed with PBS three times.

Cytotoxic activities experiment in vitro

The dark toxicity and phototoxicity of ZnPc-PYR were detected using 4T1 and HeLa cells by the MTT assay under hypoxic or normoxia conditions. Cells were cultured in 96-well plates until monolayers were spread at the bottom of the well. The original medium was discarded and photosensitizers solution ([ZnPc-PYR] = 6 μM) or serum-free medium (control group) were added. After incubation for 4 hours, the cells were irradiated under 665 nm laser (1 W·cm^{-2}) for 4 min, 808 nm laser (1 W·cm^{-2}) for 4 min, and 665+808 nm (665 nm laser irradiation for 4 min before 808 nm laser irradiation for 4 min), cells that studied dark toxicity have been grown in the dark.

The toxicity of ZnPc-PYR to HeLa cells under hypoxic or normoxia conditions was also studied using an apoptosis assays kit (Annexin V/FITC-PI) according to the directions. The cells were colocalized with ZnPc-PYR (6 μM) for 4 h and irradiated under 665 nm LED for 10 min, 808nm LED for 20 min, and 665 + 808 nm (665 nm LED irradiation for 10 min before 808 nm LED irradiation for 20 min). After incubation for 24 h at 37 °C, all HeLa cells in the Cell Culture Plates were collected and resuspended in 200 μL of binding buffer. The cells were stained with 2.5 μL Annexin V and 5 μL PI at 4 °C in the dark for 20 min. Cell apoptosis was detected by flow cytometry.

In the MTT or apoptosis experiment under hypoxic conditions, the cells were administered with the medium deoxygenated with nitrogen, and the cells have been cultured in a hypoxic incubator (1% O_2, 5 % CO_2, 37 °C).

Anticancer activity in vivo

Female BALB/c mice bearing 4T1 tumors were divided into five groups to investigate the therapeutic effect of PDT on ZnPc-PYR in vivo: 1) saline alone; 2) 665 nm LED + 808 nm laser; 3) ZnPc-PYR + 665 nm LED; 4) ZnPc-PYR + 808 nm laser; 5) ZnPc-PYR + 665 nm LED + 808 nm laser (665 nm LED : 0.9 W cm^{-2} , 30 min ; 808 nm laser : 0.3 W cm^{-2} , 7 min). From day 0, the BALB/c mice were intravenously injected with ZnPc-PYR (5 mg kg^{-1}), followed by irradiation after 6 h. The tumor size was measured every day and calculated by the following formula

$$v = \left(d^2 \times l\right) \div 2$$

where *d* was the tumor's width, and *l* was the tumor's length. The body weights of the mice were also recorded. PDT therapeutic effect was also examined by H&E staining of the tumor and significant

organ slices in mice.

Verification of 808nm deeper penetration depth

Anticancer activity in vivo Female BALB/c mice bearing 4T1 tumors were divided into two groups to investigate the therapeutic effect of PDT on ZnPc-PYR in vivo: 1) saline alone; 2) ZnPc-PYR + 1.5 cm pork + 808 nm laser. From day 0, the BALB/c mice were intravenously injected with ZnPc-PYR (5 mg kg^{-1}), followed by irradiation after 6 h (808 nm laser: 0.3 $W{\cdot}cm^{-2}$, 7 min). When irradiation is performed every day, a piece of pork muscle tissue with an average thickness of 1.5 cm is placed in front of the 808 nm excitation light source to simulate the treatment of deep tumors. The tumor size was measured every day.

Cytotoxic activities experiment in vitro Cells were cultured in 96-well plates until monolayers were spread at the bottom of the well. The original medium was discarded and photosensitizers solution ([ZnPc-PYR] = 6 μM) or serum-free medium (control group) were added. After incubation for 4 hours, the cells were irradiated under 665 nm laser (1 $W{\cdot}cm^{-2}$) for 4 min, 808 nm laser (1 $W{\cdot}cm^{-2}$) for 4 min, during irradiation, a piece of pork muscle tissue with an average thickness of 1.5 cm is placed in front of the 808 nm excitation light source to simulate deep tumor treatment.

The endocytosis pathways of ZnPc-PYR in the presence CrEL

Phthalocyanine stock solution was diluted to 6 μM with DMEM without phenol red and detect the absorbance A1 at the characteristic absorption peak. HeLa cells were cultured in 24-well plates with DMEM containing 10 % NBS. After incubating overnight, add 500 μL of PBS solution to each well to wash twice, the cells were colocalized with ZnPc-PYR (6 μM) for 4 h at 4 °C, transfer the upper solution into a micro cuvette, and measure the absorbance A2 of the sample at the characteristic absorption peak of phthalocyanine. Use the following formula to calculate the uptake rate *W*.

HeLa cells were cultured in 24-well plates with DMEM containing 10 % NBS. After incubating overnight, add 500 μL of PBS solution to each well to wash twice, the cells were colocalized with different endocytosis inhibitors ([Chlorpromazine] = 2 μM; [Nystatin] = 2.5 μg/mL; [Amiloride] = 100 μM). HaLa cells were incubated with these inhibitors for one hour before incubation with ZnPc-PYR for 4 hours. Transfer the upper solution into a micro cuvette, and measure the absorbance A2 of the sample at the characteristic absorption peak of phthalocyanine. The uptake rate *W* was calculated according

to the following equation.

$$W = (A_1 - A_2) \div A_1 \times 100\%$$

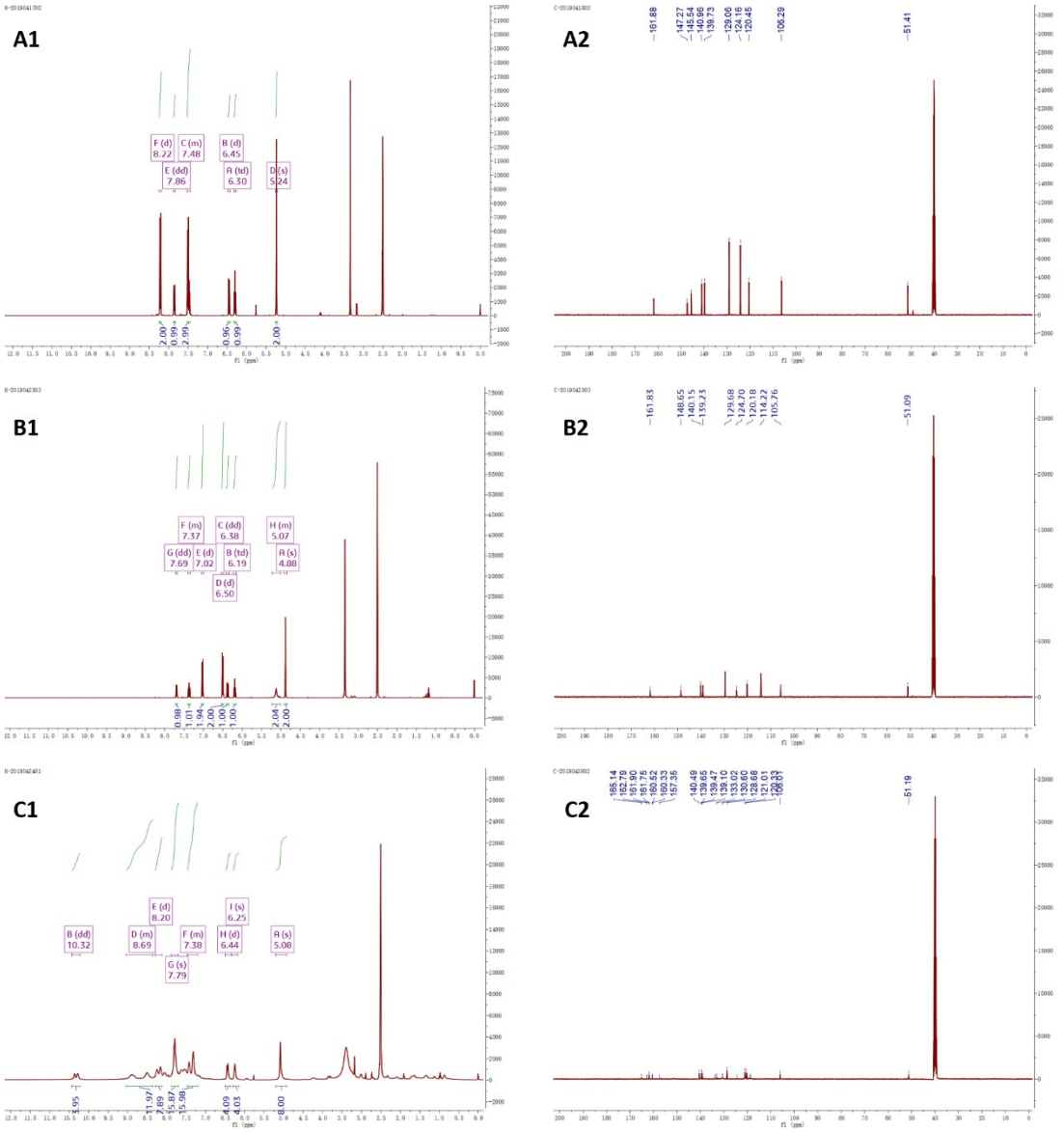

Fig. S3. The ^{1}H NMR spectrum (A1) and ^{13}C NMR spectrum (A2) of 1-(4-nitrobenzyl) pyridin-2(1H)-one; ^{1}H NMR spectrum (B1) and ^{13}C NMR spectrum (B2) of 1-(4-aminobenzyl) pyridin-2(1H)-one; ^{1}H NMR spectrum (C1) and ^{13}C NMR spectrum (C2) of ZnPc-PYR.

The TEM image indicated that in an aqueous solution, ZnPc-PYR aggregates into ultra-small nanoparticles (< 5 nm). Then the ultra-small nanoparticles clustered into loose clusters. Phthalocyanines possess highly conjugated 18 π-electron planar aromatic systems and tend to aggregate in the face-to-face form (H-form aggregator) by π-π stacking interaction. The modified 2-pyridones were in the side chains of phthalocyanine. Thus, after forming the aggregators, the 2-

pyridones are in the peripheral position, helping its $^1O_2$ storage and releases functions. Besides, some ultra-small nanoparticles clustered into loose clusters in an aqueous solution. The diameter of O_2 is only about 0.3 nm [2]. The cluster is loose to ensure O_2 and $^1O_2$ can penetrate freely post light irradiation. Thus, the photosensitizers do not need to be released after cellular internalization and can effectively capture and release the $^1O_2$ to oxidize biomacromolecules inside cells.

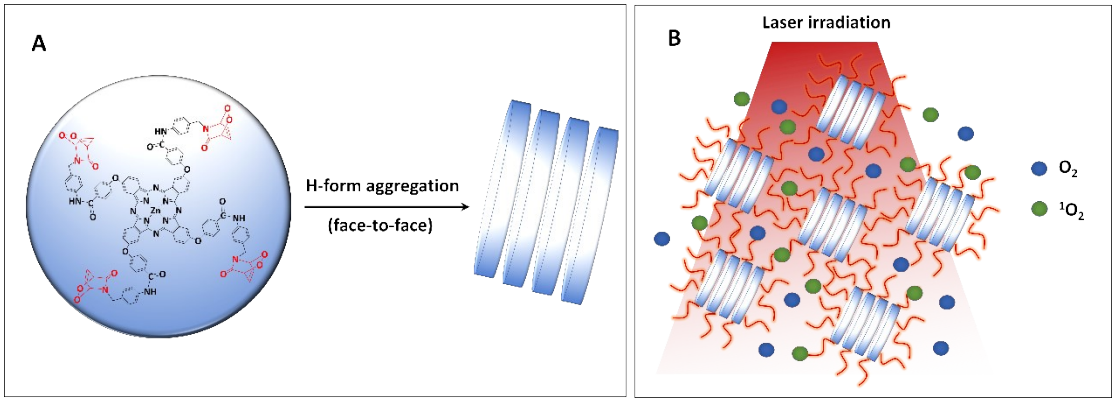

Scheme S1. The aggregation style of ZnPc-PYR and the capture and release the $^1O_2$ process in the loose cluster post light irradiation.

ZnPc-PYR has low water solubility and is easy to H-form aggregator (face-to-face aggregator) form in water because a prominent H-aggregator peak was detected in its absorbance spectra [3]. The added CrEL can be attached to the ZnPc-PYR nanoparticles' surface to increase their dispersion ability (Figure S4 A1). Thus, we choose the minimum CrEL amount to obtain the satisfactory stable dispersion ability to avoid the extra side effect from the CrEL. The content ratio between the ZnPc-PYR and CrEL was 1:0.946 (mg/mg) in our system.

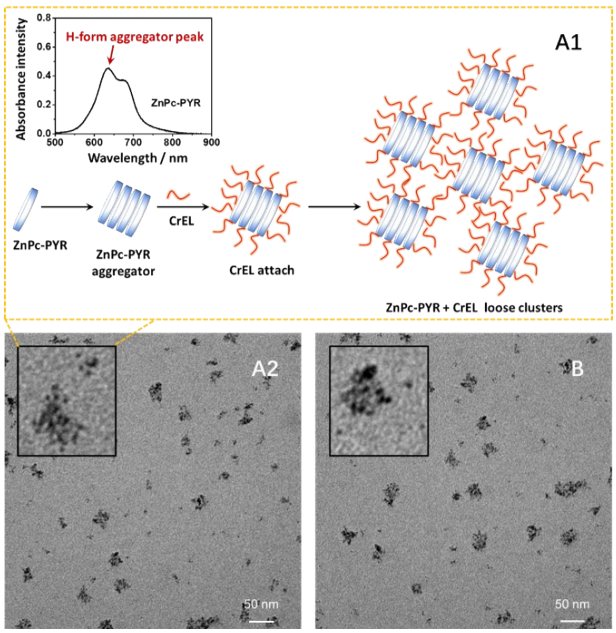

Fig. S4 TEM image of ZnPc-PYR in the presence CrEL at day 1 in aqueous solutions (A1), ZnPc-PYR aggregation schematic presentation (A2) and TEM image of ZnPc-PYR in the presence CrEL at day 7 in aqueous solutions (B).

Besides, we studied the morphology and stability of the ZnPc-PYR in the presence CrEL. The TEM image indicated that ZnPc-PYR aggregates into ultra-small nanoparticles (< 5 nm). Then the ultra-small nanoparticles clustered into loose clusters (Figure S4 A). After 7 days, no apparent morphology and dispersion ability change were detected (Figure S4 B). The data indicated that the ZnPc-PYR in the presence CrEL could stable for 7 days in an aqueous solution.

As shown in Figure S5 A, after adding CrEL, the fluorescence intensity of ZnPc-PYR was increased. Besides, in the presence of CrEL, the $^1O_2$ generation capacity of ZnPc-PYR is significantly enhanced. According to the method in the literature [4], MB was used as the standard sensitizer under 665 nm laser irradiation condition, the $^1O_2$ quantum yield (φ) of MB under 665 nm laser irradiation was 52 % [5, 6], the $^1O_2$ quantum yield of ZnPc-PYR increased from 7.127 % to 15.872 % under the excitation of 665 nm light. Similarly, under 808 nm laser irradiation conditions, ICG was used as the standard sensitizer, the $^1O_2$ quantum yield (φ) of ICG under 808 nm laser irradiation was 0.2 % [4, 7], the $^1O_2$ quantum yield of ZnPc-PYR increased from 2.408 % to 3.135 % under the excitation of 808 nm light. We also compared the phototoxicity of ZnPc-PYR on HeLa cells in the presence of CrEL under the excitation of 665 nm and 808 nm light. The MTT assay results show that the PDT activity of ZnPc-PYR in the presence CrEL is

significantly enhanced. The above data fully reflects the superiority of the ZnPc-PYR in the presence CrEL.

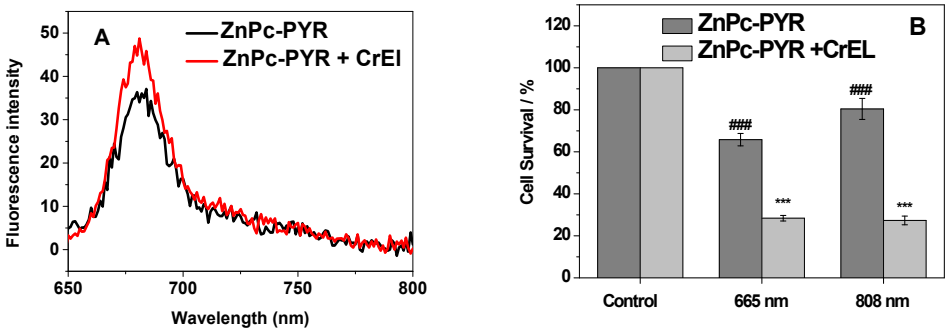

Fig. S5 (A) The fluorescence intensity changing of ZnPc-PYR before and after adding CrEL; (B) photo-induced toxicity changing of ZnPc-PYR before and after adding CrEL post 665 or 808 nm light irradiation. (Data are expressed as means ± SD; *P < 0.05; **P < 0.01 ***P < 0.001 versus control; #P < 0.05; ##P < 0.01 ###P < 0.001 versus add CrEL group.)

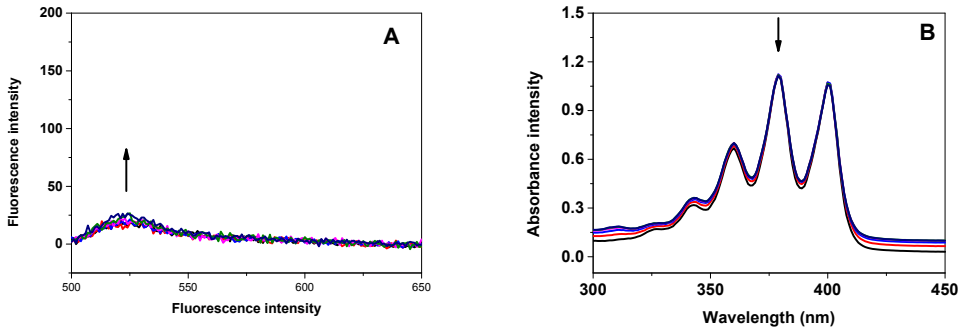

Fig. S6. The total ROS (A) and $^1O_2$ (B) generation in aqueous solution of ICG (1 μM) post 808 nm light irradiation (0.25 W cm^{-2}, the fluorescence signal intensity of DCFH was detected once every 30 s and the 378 nm absorbance intensity decreasing of ADPA was monitored once every 2 min).

Firstly, the cellular uptake of ZnPc-PYR in the presence CrEL into HeLa cells at 4 °C and 37 °C was compared. Under the condition of 4 °C, the cells showed significant uptake inhibition of ZnPc-PYR in the presence CrEL, indicating the nanoformulation is taken up by cells through endocytosis. Endocytosis is a process that requires energy. In a low-temperature environment, cells need the energy to maintain their growth. When energy is insufficient, endocytosis will be inhibited [8]. There are three pathways of endocytosis, including clathrin-dependent endocytosis, caveolin-dependent endocytosis, and

macropinocytosis. The chlorpromazine, amiloride and nystatin were used as clathrin-mediated endocytosis, macropinocytosis and caveolae-mediated endocytosis pathway inhibitor, respectively [9-12]. As shown in Figure S7, chlorpromazine has no inhibitory effect on the uptake of ZnPc-PYR in the presence CrEL. In contrast, nystatin, amiloride have a specific inhibitory effect on the uptake of drugs by tumor cells, which shows that ZnPc-PYR in the presence CrEL is taken up by cells through endocytosis mediated by caveolae and macropinocytosis.

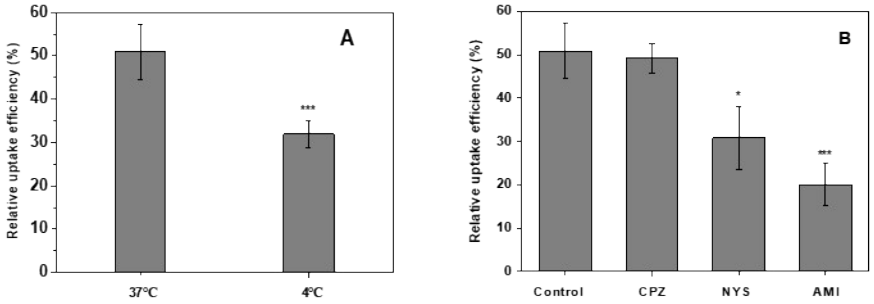

Fig. S7. (A) Uptake rate of ZnPc-PYR by HeLa cells at 4 °C and 37 °C. (B) Uptake of ZnPc-PYR by HeLa cells under the action of endocytosis inhibitor ([Chlorpromazine] = 2 μM; [Nystatin] = 2.5 μg/mL; [Amiloride] = 100 μM). (Data are expressed as means ± SD; *P < 0.05; **P < 0.01 ***P < 0.001 versus control.)

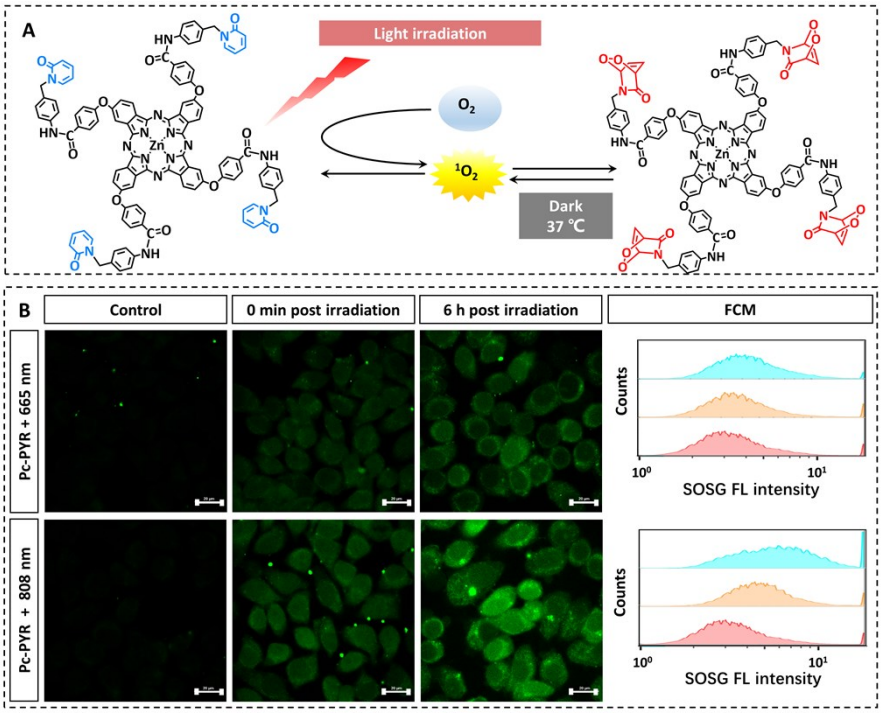

Fig. S8. (A) The schematic presentation of the $^1O_2$ storage and release mechanism of ZnPc-PYR. (B) In

vitro $^1O_2$ generation, storage, and release of ZnPc-PYR post 665 or 808 nm light irradiation and dark incubation (bar = 20 μm).

The $^1O_2$ storage and release detection used ADPA as a $^1O_2$ sensor. As shown in the Figure S9, ADPA is bleached by $^1O_2$ to its corresponding endoperoxide. The reaction was monitored spectrophotometrically by recording the decrease in absorbance intensity at 378 nm (λ_{max} of ADPA) [13]. Like the endoperoxide of ZnPc-PYR, ADPA endoperoxide can release $^1O_2$ to induce the ADPA absorbance part to recover under the heating condition in the dark. Besides ADPA, SOSG is a commercial specific $^1O_2$ sensor. However, its detection mechanism has also based the reaction with $^1O_2$ to form an endoperoxide to enhance fluorescence intensity [14]. Thus, the slight signal recovery could not be avoided during the $^1O_2$ storage and release detection of ZnPc-PYR.

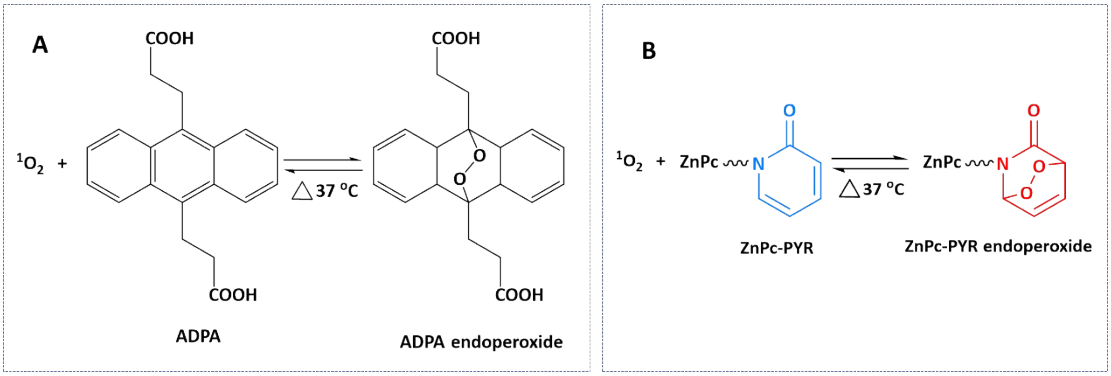

Fig. S9. The $^1O_2$ storage and release mechanism of ADPA (A) and ZnPc-PYR (B).

Just as presented in our original paper, to verify ZnPc-PYR is essential for the storage and release of $^1O_2$, we synthesized phenyl-modified ZnPc-BZA as a negative control. For ZnPc-BZA, the absorption peak of ADPA at 378 nm decrease can only be detected under the light irradiation cycle. In the dark incubation cycle (37 °C) of ZnPc-BZA, the absorption intensity decrease was not observed, but an increase in the absorption value was observed. ADPA can be oxidized by $^1O_2$ to its endoperoxide formation to store $^1O_2$ and induce its absorbance to decrease. The $^1O_2$ release from the endoperoxide formation to revert to ADPA induced the above absorption enhancement phenomenon. However, the released $^1O_2$ from the endoperoxide formation is not enough to oxidize ADPA. In contrast, for ZnPc-PYR, the absorption peak of ADPA at 378 nm decrease can be detected under the light irradiation cycle (665 nm light irradiation) and dark incubation cycle. Therefore, for ZnPc-PYR, under dark reaction conditions, the absolute value of the decrease in the absorbance value of ADPA should be added to the

value of the increase in the absorbance value caused by the structure of ADPA itself. The broken red line in the revised Fig. S10 is the data after our refitting. The $^1O_2$ release of ZnPc-PYR under dark reaction conditions accounts for 22.52 % of the total $^1O_2$ release during the entire cycle.

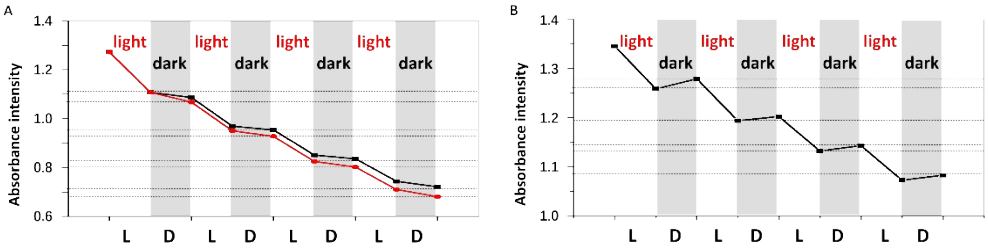

Fig. S10. ADPA bleaching in the aqueous solution of ZnPc-PYR (A) (dark line: $^1O_2$ release measured in the experiment; red line: $^1O_2$ release after refitting) or ZnPc-BZA (B) in the light cycle post 665 nm light irradiation and dark cycle.

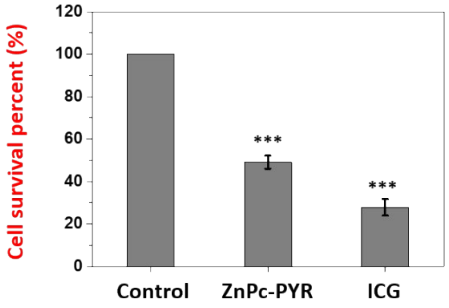

Fig. S11. The photo-induced toxicity comparison between ZnPc-PYR and ICG post 808 nm light irradiation ([ZnPc-PYR] = [ICG] = 6 μM, 808 nm laser power density =1 W cm^{-2}, light irradiation time = 2 min) (Data are expressed as means ± SD; *P < 0.05; **P < 0.01 ***P < 0.001 versus control).

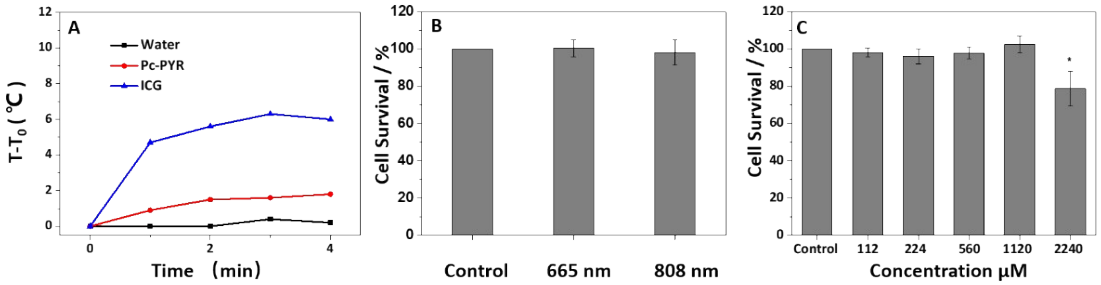

Fig. S12. (A) The temperature-rising curves of water, ZnPc-PYR and ICG ([ZnPc-PYR] = [ICG] = 6 μM) under 808 nm laser (1 W cm^{-2}) irradiation. (B) The cell survival of HeLa cells co-incubated with 6 μM ZnPc-PYR and received 1 W cm^{-2} 665 and 808 nm laser irradiation for 4 min in the absence of 1.12 mM

ascorbic acid. (C) Dark cytotoxicity evaluation of ascorbic acid (Data are expressed as means ± SD; *P < 0.05; **P < 0.01 ***P < 0.001 versus control).

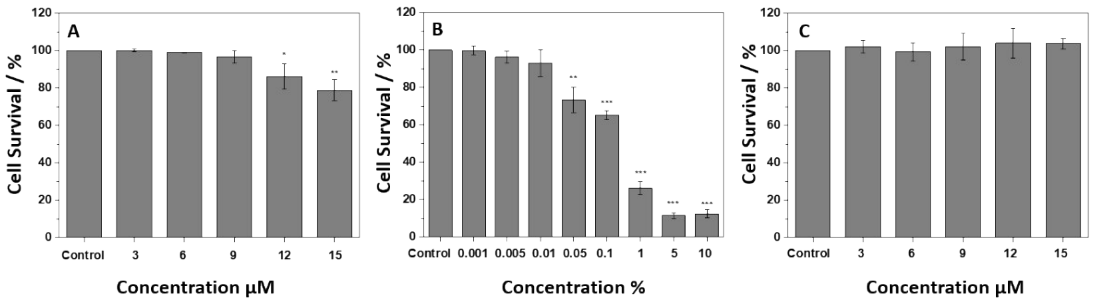

Fig. S13. Dark cytotoxicity evaluation of ZnPc-PYR (A), CrEL (B), ICG (C) on HeLa cells (Data are expressed as means ± SD; *P < 0.05; **P < 0.01 ***P < 0.001 versus control).

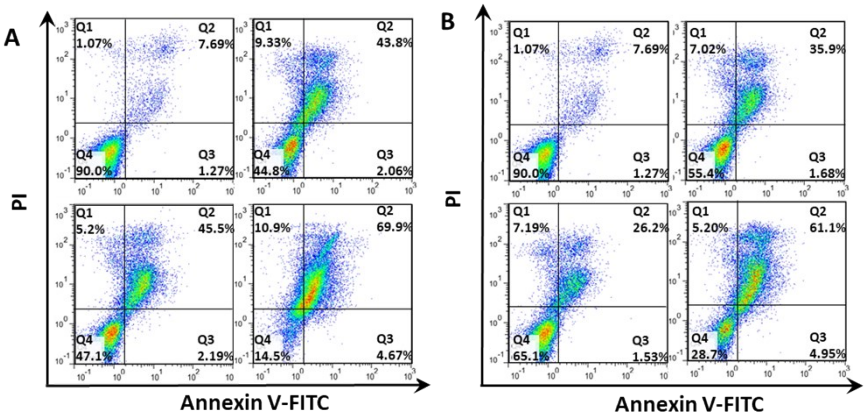

Fig. S14. The FCM data for apoptosis detection for various group under normoxic (A) and hypoxic (B) conditions.

As shown in Figure S15, the MTT assay was used to re-evaluate the anti-tumor activity of ZnPc-PYR in vitro under dual-wavelength excitation. The results showed that the PDT activity of 665 nm + 808 nm treatment group in vitro was higher than that of the single-wavelength light treatment group.

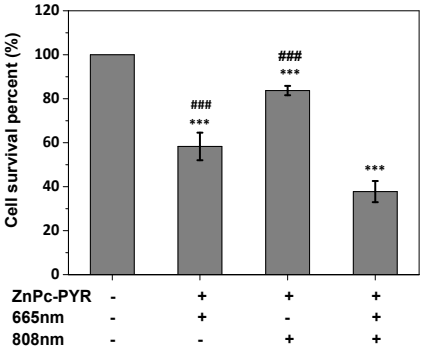

Fig. S15. Cancer cell kill capability of ZnPc-PYR post various kinds of light irradiation treatments under normoxic conditions in HeLa cells (665 nm laser: 1 W cm^{-2}, 40 s; 808 nm laser: 1 W cm^{-2}, 40 s). (Data are expressed as means ± SD; *P < 0.05; **P < 0.01 ***P < 0.001 versus control; #P < 0.05; ##P < 0.01 ###P < 0.001 versus ZnPc-PYR + 665 + 808 nm group).

For the in vitro experiment, as shown in Figure S16, in the pork's presence, 665 nm laser irradiation-induced PDT activity of ZnPc-PYR was slight. On the contrary, in the pork's presence, 808 nm laser irradiation-induced PDT activity of ZnPc-PYR was apparent.

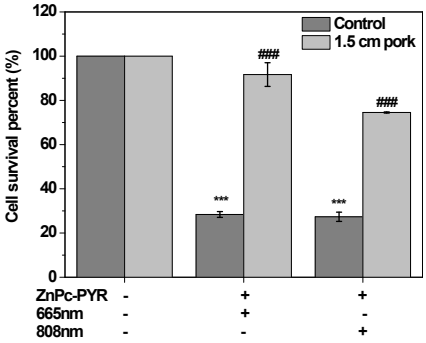

Fig. S16. In vitro ZnPc-PYR PDT activity comparison of been excited by 665 or 808 nm with or without pork (Data are expressed as means ± SD; *P < 0.05; **P < 0.01 ***P < 0.001 versus control; #P < 0.05; ##P < 0.01 ###P < 0.001 versus without pork group).

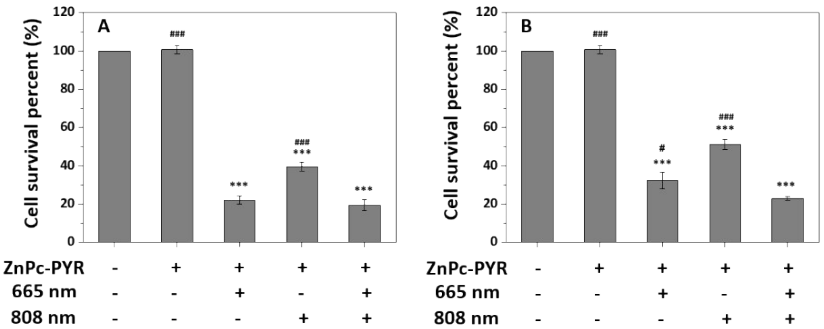

Fig. S17. The photo-induced toxicity of ZnPc-PYR (6 μM) in 4T1 cells under various kinds of light irradiation (1 W cm^{-2}, 4 min) under normoxic (A) and hypoxic (B) conditions (Data are expressed as means ± SD; *P < 0.05; **P < 0.01 ***P < 0.001 versus control; #P < 0.05; ##P < 0.01 ###P < 0.001 versus ZnPc-PYR + 665 + 808 nm group).

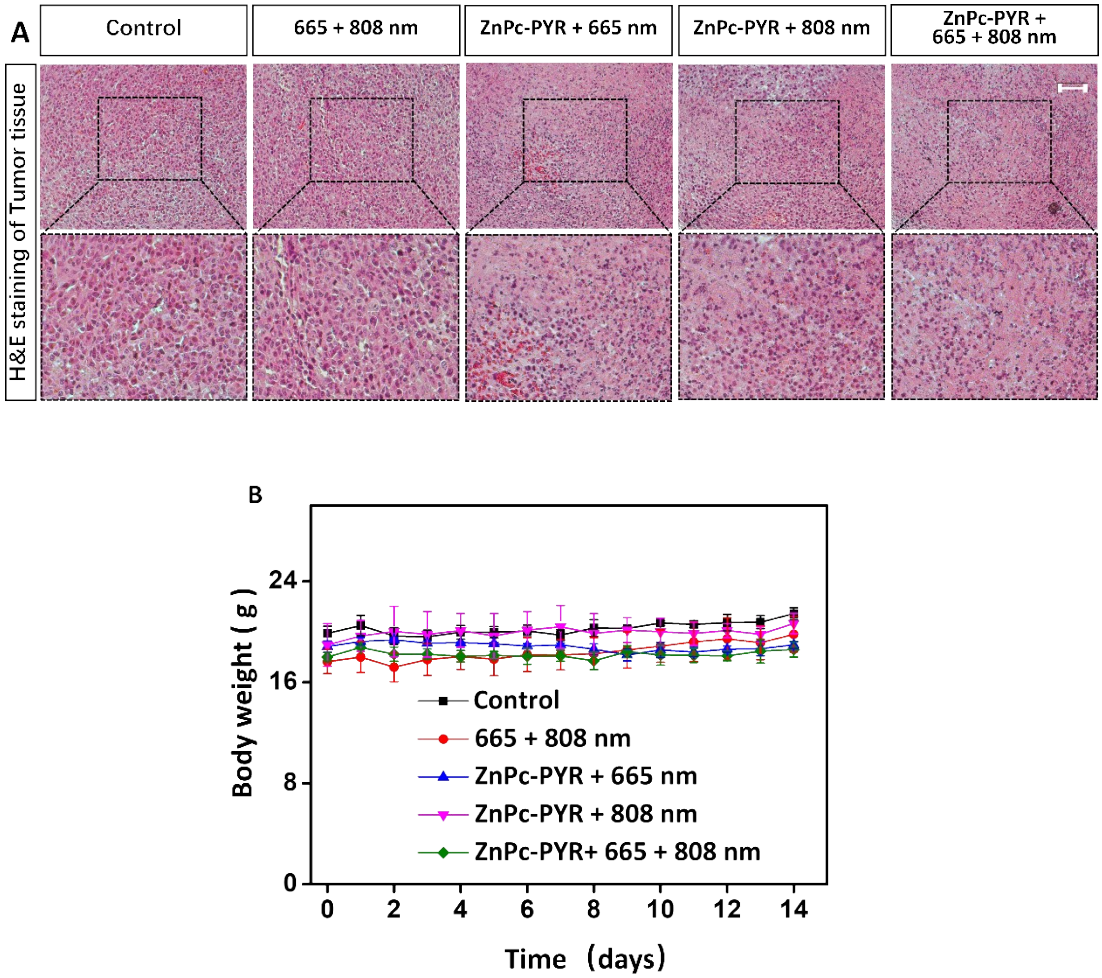

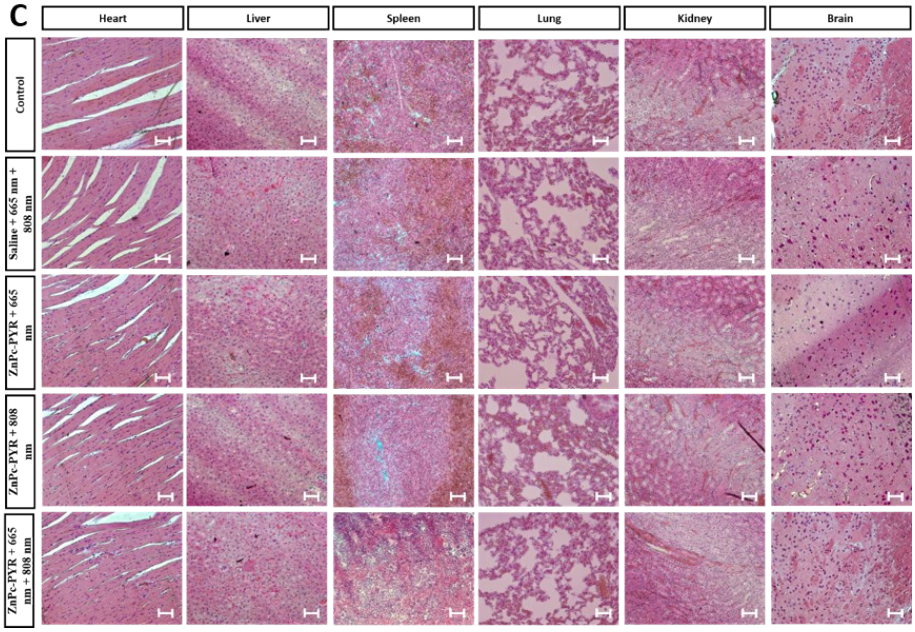

Fig. S18. H&E staining of tumor tissue ultrathin sections of various groups (A); mice weight changes post 14 days of various treatments (B) and H&E staining of major tissue sections of the mice during 14 days of ZnPc-PYR treatment under various light irradiation condition (C). (bar = 50 μm).

For the in vivo experiment, as shown in Figure S19, the experimental results show that although the application of 1.5 cm thick pork muscle tissue will reduce the anti-tumor activity in the ZnPc-PYR + 808 nm group, it also can still significantly inhibit the growth of mouse tumors during 14 days of treatment. The above added new data verified that the deep PDT effect of ZnPc-PYR.

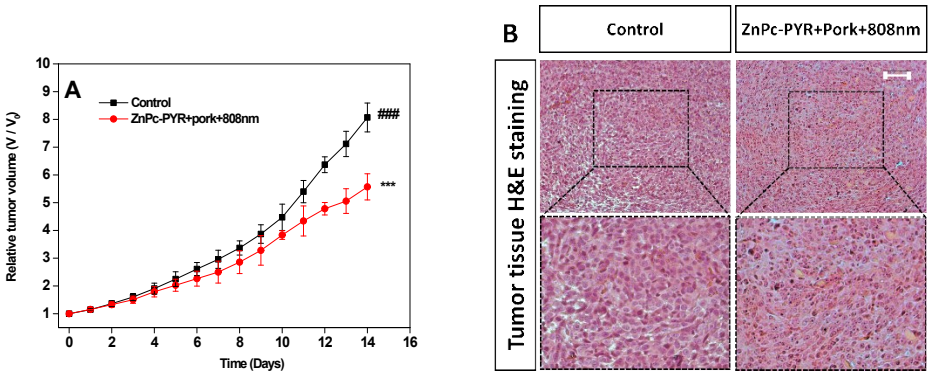

Fig. S19. (A) Tumor volume changes post 14 days of various treatment. (B) H&E staining of tumor tissue ultrathin sections of the two groups (bar = 50 μm) (Data are expressed as means ± SD; *P < 0.05; **P < 0.01 ***P < 0.001 versus control; #P < 0.05; ##P < 0.01 ###P < 0.001 versus treatment group).

Notes and references

1. T. Wang, J. Hu, Small, 2018, **14**, e1802337.
2. W. M. Vaughan and G. Weber, Biochemistry, 1970, **9**, 464-473.
3. A. Wang, L. Gui, S. Lu, Dyes and Pigments, 2016, **126**, 239-250.
4. Q. Wang, J. Xu, R. Geng, Biomaterials, 2020, **231**, 119671.
5. A. Kamkaew, S. H. Lim, H. B. Lee, Chem. Soc. Rev., 2013, **42**, 77-88.
6. N. Adarsh, M. Shanmugasundaram, R. R. Avirah, Chemistry, 2012, **18**, 12655-12662.
7. Y. Dai, J. Su, K. Wu, ACS Appl Mater Interfaces, 2019, **11**, 10540-10553.
8. S. L. Schmid and L. L. Carter, The Journal of Ceil Biology, 1990, **111,** 2307--2318
9. S. Mayor and R. E. Pagano, Nat Rev Mol Cell Biol, 2007, **8**, 603-612.
10. D. Vercauteren, R. E. Vandenbroucke, A. T. Jones, Mol. Ther., 2010, **18**, 561-569.
11. N. Nagai, F. Ogata, H. Otake, Int. J. Nanomedicine., 2019, **14**, 1213-1227.
12. W. Dejonghe, S. Kuenen, E. Mylle, Nat. Commun., 2016, **7**, 11710.
13. I. Roy, T. Y. Ohulchanskyy, H. E. Pudavar, Journal of the American Chemical Society, 2003, **125**, 7860–7865.
14. T. Kiesslich, A. Gollmer, T. Maisch, Biomed Res Int, 2013, 840417.